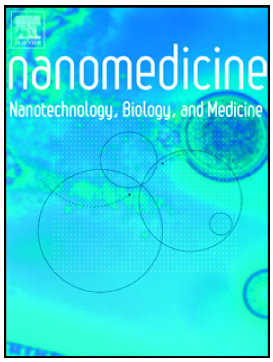

Encapsulation in lipid-core nanocapsules improves topical treatment with the potent antileishmanial compound CH8

Douglas O Escrivani, Milene Valéria Lopes, Fernanda Poletto, Stela Regina Ferrarini, Ariane J. Sousa-Batista, Patrick G. Steel, Sílvia Stanisçuaski Guterres, Adriana Raffin Pohlmann, Bartira Rossi-Bergmann

PII: S1549-9634(19)30205-9

DOI: https://doi.org/10.1016/j.nano.2019.102121

Reference: NANO 102121

To appear in: *Nanomedicine: Nanotechnology, Biology, and Medicine*

Revised date: 1 August 2019

Please cite this article as: D.O. Escrivani, M.V. Lopes, F. Poletto, et al., Encapsulation in lipid-core nanocapsules improves topical treatment with the potent antileishmanial compound CH8, *Nanomedicine: Nanotechnology, Biology, and Medicine*(2019), https://doi.org/10.1016/j.nano.2019.102121

ORIGINAL RESEARCH

Encapsulation in lipid-core nanocapsules improves topical treatment with the potent antileishmanial compound CH8.

Douglas O Escrivani[a,1], Milene Valéria Lopes[a,1], Fernanda Poletto[b], Stela Regina Ferrarini[c], Ariane J. Sousa-Batista[a], Patrick G. Steel[d], Sílvia Stanisçuaski Guterres[c], Adriana Raffin Pohlmann[b], Bartira Rossi-Bergmann[a]*

[a]Instituto de Biofísica Carlos Chagas Filho, Universidade Federal do Rio de Janeiro, RJ, Brazil;

[b]Departamento de Química Orgânica e Programa de Pós-Graduação em Química, Instituto de Química, Universidade Federal do Rio Grande do Sul, Porto Alegre, RS; Brazil;

[c]Programa de Pós-Graduação em Ciências Farmacêuticas, Universidade Federal do Rio Grande do Sul, Porto Alegre, RS, Brazil.

[d] Department of Chemistry, Durham University, UK

[1] These authors contributed equally to this work

[*] **Corresponding author:** Bartira Rossi-Bergmann
Instituto de Biofísica Carlos Chagas Filho, Universidade Federal do Rio de Janeiro, CCS, Av. Carlos Chagas Filho 373, CEP 21941-902, Rio de Janeiro, RJ, Brazil.
Tel.: +55 21 2260 6963.

E-mails: douglas@biof.ufrj.br (D.O., Escrivani), milevaleria@yahoo.com.br (M.V. Lopes), fernanda.poletto@ufrgs.br (F. Poletto), stelaferrarini@ufmt.br (S.R. Ferrarini), adriana.pohlmann@ufrgs.br (A. R. Pohlmann), silvia.guterres@ufrgs.br (S.S. Guterres), bartira@biof.ufrj.br (B. Rossi-Bergmann).

Word count - Abstract: 147

Word count - Complete ms: 5044

References: 47

Figures: 6

Tables: 2

Competing financial interest: The authors declare no competing financial interests.

Funding source: We thank the Brazilian agencies CAPES, CNPq, and FAPERGS for financial support of this project and The Royal Society London for an International Collaboration Award for Research Professors (#IC160044 to BRB and PGS).

.

ABSTRACT

Cutaneous leishmaniasis (CL) is a neglected parasitic disease conventionally treated by multiple injections with systemically toxic drugs. Aiming at a more acceptable therapy, we developed lipid-core nanocapsules (LNC) entrapping the potent antileishmanial chalcone (CH8) for topical application. Rhodamine-labeled LNC (Rho-LNC-CH8) was produced for imaging studies. LNC-CH8 and Rho-LNC-CH8 had narrow size distributions (polydispersity index < 0.10), with similar mean sizes (~180 nm) by dynamic light scattering. *In vitro*, Rho-LNC-CH8 were rapidly internalized by extracellular *Leishmania amazonensis* parasites macrophages in less than 15 minutes. LNC-CH8 activated macrophage oxidative mechanisms more efficiently than CH8, and was more selectively toxic against the intracellular parasites. *In vivo*, topically applied Rho-LNC-CH8 efficiently permeated mouse skin. In *L. amazonensis*-infected mice, LNC-CH8 reduced the parasite load by 86% after three weeks of daily topical treatment, while free CH8 was ineffective. In conclusion, LNC-CH8 has strong potential as a novel topical formulation for CL treatment.

Keywords: Leishmaniasis, nitrochalcone, lipid-core nanocapsules, drug delivery, skin, topical treatment.

BACKGROUND

Cutaneous leishmaniasis (CL) is the most common clinical form of the disease, accounting for an estimated 1.2 million cases per year, mainly in developing countries[1]. After inoculation of flagellated promastigotes into the skin by blood-feeding sandflies, successful parasites invade dermal macrophages, transform into amastigote forms, and survive and multiply intracellularly by downregulating host cell defense mechanisms such as the production of reactive oxygen species (ROS) and nitric oxide (NO), and proteolytic digestion inside the parasitophorous vacuole[2]. Chronic and disfiguring ulcers develop at the infection site, and may spread to other parts of the skin.

Although the infection is limited to the skin, current CL chemotherapy involves long-term intravenous or intramuscular injections with pentavalent antimonials (Pentostam® or Glucantime®), pentamidine or amphotericin B. The injections are painful, systemically toxic and result in high hospital costs.[3] The only oral antileishmanial drug – miltefosine – is used mostly for visceral leishmaniasis in the Old World, and is not approved for use in New World countries such as Brazil. To circumvent these difficulties, an effective topical treatment is the obvious choice for CL. However, creams containing paromomycin, miltefosine and amphotericin B have shown partial or no efficacy against CL, in particularly against New World *Leishmania* species[4-6]. Failure of topical formulations is typically linked to poor skin permeation, mainly to high drug molecular size and/or inappropriate lipophilicity[7]. The addition of strong permeation enhancers to topical formulations allows drugs to reach the deep dermis; however, most permeation enhancers cause unacceptable irritation at

the treatment site[8]. Thus, the present scenario justifies the search for new antileishmanial agents and formulations, particularly for topical CL treatment.

Due to the inadequacy of current CL chemotherapy, the Drugs for Neglected Disease initiative (DNDi) has supported the search for new topical or oral treatments for CL that are efficacious against all species, easy to administer, can be given in as a short treatment course (14-28 days), and are compatible with combination therapy and adapted to tropical climates[9]. We have previously reported the strong antileishmanial activity and selectivity of the synthetic chalcone CH8[10] (3-nitro-2-hydroxy 4,6-dimetoxychalcone, Figure 1), a lipophilic and highly stable compound that fulfills most of the criteria specified by DNDi for a promising anti-leishmanial drug. *In vivo*, CH8 given to mice by the oral route is effective and safe against both cutaneous and visceral leishmaniasis[11]. Importantly, local subcutaneous injections with CH8 either in the free form[10] or loaded in slow-release systems[12, 13] effectively treated mice with CL. However, effective topical formulations remain a challenge for this and other anti-leishmanial compounds.

Drug nanocarriers have been extensively applied to improve drug delivery and bioavailability of molecules with poor solubility in water, such as chalcones. These systems may protect the drug against degradation while promoting its intestinal uptake or skin permeation through the epidermis layer or hair follicle[14]. Lipid-core nanocapsules (LNCs) made with a biodegradable poly(ε-caprolactone) shell have emerged as appropriate nanocarriers to increase the bioavailability of lipophilic agents, since these can be entrapped into the carrier lipid core[15]. Previously, we showed that encapsulation in LNC promotes the intestinal absorption of the flavonoid quercetin, increasing by 40

fold the efficacy of this lipophilic molecule via the oral route, in a murine model of CL.[16] In topical drug delivery assays, LNCs successfully promoted skin permeation of other lipophilic molecules such vitamin K1, resveratrol and curcumin[17, 18], without appreciable skin irritation.

Given the efficacy of CH8 against CL and the safety and potential of LNCs as nanocarriers of drugs to the skin, we describe here the development and testing – both *in vitro* and *in vivo* - of an LNC-CH8 formulation for the topical treatment of CL.

METHODS

Animals and ethics statement

BALB/c mice (female, eight-week-old, 23 g) used in the experiments were maintained under controlled conditions at the animal facilities of the Federal University of Rio de Janeiro (UFRJ, RJ, Brazil).

The animal protocols used in this study were approved by the local Animal Care and Use Committee (protocol number CAUAP118). All animal experiments were conducted in compliance with the principles stated in the *Guide for the Care and Use of Laboratory Animals, 8th Edition.*[19]

Production of lipid-core nanocapsules

The compound 3-nitro-2-hidroxy-4,6-dimethoxy chalcone (CH8, Figure 1) was synthesized as described previously[10].

Lipid-core nanocapsules (LNC) were prepared by a self-assembly methodology[20]. Briefly, 200 mg poly(ε-caprolactone) (80,000 g mol^{-1} PCL;

Sigma-Aldrich Co., USA), 80 mg sorbitan monostearate (Sigma-Aldrich Co.), 310 mg capric/caprylic triglyceride (Alpha Quimica, Brazil) were dispersed in acetone (46 mL), and then injected into an aqueous phase composed of polysorbate 80 (185 mg; Gerbras, Brazil), ethanol (8 mL) and water (106 mL). The mixture was stirred for 10 minutes at room temperature, the solvent was evaporated under reduced pressure (rotatory evaporator, Büchi, Switzerland) at 40 ^{0}C and the aqueous suspension was concentrated for a final volume of 10 mL. Streptomycin (100 µg/mL) and penicillin (100 UI/mL) (Sigma-Aldrich Co.) were added. LNC-CH8 was prepared by adding 5 mg CH8 in the organic phase and Rho-LNC-CH8 was prepared as described above, with the exception that part of the unlabeled PCL was replaced with 10 mg of Rhodamine B-labeled PCL (Rho-PCL)[21].

Characterization of lipid-core nanocapsules

Formulations were analyzed by laser diffraction, in a Mastersizer® 2000 particle size analyzer (Malvern, UK)[15], to determine their volume-weighted mean diameter (D[4,3]). Size polydispersity was calculated considering the diameters at 10%, 50%, and 90% of the cumulative size distribution (SPAN). The Z-average diameter (method of cumulants) and polydispersity index were determined by photon correlation spectroscopy (PCS) using a Zetasizer Nano ZS particle analyzer (Malvern, UK) after dilution. The zeta potential of nanoparticles was calculated by examining the electrophoretic mobility of formulations dispersed in a 10mM NaCl aqueous solution (pH = 7.0) using a Zetasizer Nano ZS (Malvern, UK).

CH8 encapsulation efficiency

A sample of the formulation was dissolved in acetonitrile and filtered (0.45 µm, Merck Millipore, USA). The CH8 content was quantified by HPLC-UV [Perkin-Elmer® S200 pre-column, column LiChrospher 100 RP_{18} (5µm) (Merck®)], using a mobile phase of acetonitrile:aqueous 0.01% phosphoric acid (Tedia) (80:20 v/v), with a flow rate of 1 mL/min and a detection wavelength of 337 nm, as described previously.[22]

Parasites

Leishmania amazonensis (MHOM/BR/75/Josefa strain) promastigotes were maintained in culture at 26^{o}C in M199 medium (CultiLab, Brazil) supplemented with 10% heat-inactivated fetal calf serum (HIFCS) (CultiLab, Brazil), 0.2% hemin (Sigma-Aldrich Co., USA), 100 µg/mL streptomycin and 100 UI/mL penicillin (Sigma-Aldrich Co., USA), herein referred to as 'complete medium'. Alternatively, GFP-expressing parasites were cultured as described previously[23] Parasites were always used at the stationary phase of growth.

Anti-amastigote activity

Bone marrow derived macrophages (BMDM) from BALB/c mice were prepared as described[23] and plated (2x10^{5}/ well) onto circular glass coverslips in 24-well culture plates, and incubated for 24 h at 37^{o}C (and 5% CO_2). Then macrophage monolayers were kept uninfected or were infected with *L. amazonensis* promastigotes (5x10^{6} cells/ mL) for 4 h at 34^{o}C / 5% CO_2. After a further 24h of infection at 37^{o}C, macrophages were incubated with 0.1, 1, 10 and 100 µg/mL of CH8, LNC-CH8 or equivalent blank LNC concentrations, for

48h at 37°C. Then, cells were washed with PBS and stained with panoptic (Instant Prov kit, Newprov, Brazil) according to the manufacturer's instructions. The number of amastigotes in 200 cells was counted by light microscopy examination, in a Nikon Eclipse Ti microscope, at 1000 X magnification. The compound concentrations required to reduce amastigote numbers by 50% (IC_{50} values) were calculated by linear regression analysis.

Cytotoxicity

The supernatants of the anti-amastigote assay were collected at the end of the treatment described above and the release of the cytosolic enzyme lactate dehydrogenase (LDH) by the macrophages was used as a cytotoxicity indicator. For total and spontaneous LDH releases, supernatants were collected from cells cultured with 1% triton and medium alone, respectively. LDH release was measured by a colorimetric assay using the detection kit DHL (Doles, Brazil), according to the manufacturer's instructions. Readings were taken at 492 nm in PowerWave XS spectrophotometer (BIO-TEK, USA), and cytotoxicity to BMDM calculated as the % of specific LDH release = (test - spontaneous / total - spontaneous) x100. The compound concentrations required to produce 50% of cytotoxicity (CC_{50} values) were calculated by linear regression analysis. The selectivity index (SI) for each compound was calculated as the ratio between 50% cytotoxicity (CC_{50}) and 50% anti-amastigote activity (IC_{50}).

Rho-LNC-CH8 uptake assays

For Rho-LNC-CH8 uptake by promastigotes, parasites (10^6 cells/mL), were plated in 24 well-plates in M199 medium containing 10% HIFCS, in the presence or absence of Rho-LNC-CH8 (10 μg/mL CH8). After 15 and 60 min of

incubation, cells were washed with phosphate-buffered saline (PBS) and transferred to glass slides for visualization in an Eclipse-Ti fluorescence microscope (Nikon) equipped with a CFI Plan Apo Lambda 100X Oil objective. Standard filters for FITC (B-2A) or rhodamine (G2 E/C) and DIC were used. Images were analyzed using the Adobe Photoshop CC software (version 14.2.1). Alternatively, fluorescent cells were analyzed by flow cytometry in a FACScan equipment (BD Biosciences), and the results were expressed as the percentage of cells (as gated by FSC vs. SSC) with fluorescence above $6x10^0$ arbitrary units (10^5 events/sample).

For LNC-CH8 uptake by macrophages and intracellular amastigotes, BMDM ($2x10^5$ cells/well) were infected as described for the anti-amastigote activity assay. After 24 h, infected and non-infected macrophages were treated with Rho-LNC-CH8 (10 μg/mL CH8) for up to 240 min and cells were imaged by fluorescence microscopy as described above. Alternatively, BMDM were infected and treated in 6-well plates (at 10^6 cells/well), and then subjected to flow cytometry analysis as described above.

Macrophage reactive oxygen species (ROS) production

BMDM ($1x10^5$ cells/well) were plated into black, clear-bottom 96-well plates, and then infected with *L. amazonensis* promastigotes and treated with CH8, LNC-CH8, or LNC as described above for the anti-amastigote assay. Then, cells were incubated with the oxidation-sensitive fluorescent dye 2',7'-dichlorodihydrofluorescein diacetate (H_2DCFDA, at 10 μM; Invitrogen, USA) for 20 min at 37°C, and fluorescence was read at 485/528 nm (excitation/emission) in an FLX800 plate fluorimeter (BIO-TEK, USA). Uninfected and infected

macrophages incubated with 250 µg/mL Zymosan (Sigma–Aldrich Co.) were used as positive controls for ROS production.

Macrophage nitric oxide (NO) production

BMDM ($1x10^5$ cells/ well) were plated in 96-well plates, and then infected with *L. amazonensis* promastigotes and treated with CH8, LNC-CH8, or LNC as described above for the anti-amastigote assay. NO production in culture supernatants was measured by the Griess method, as described previously[24]. Readings were taken at 570 nm in a PowerWave XS spectrophotometer (BIO-TEK, USA). The nitrite concentration was calculated using a standard curve of sodium nitrite ($NaNO_2$), from 0 to 50 µM. Uninfected and infected macrophages incubated with 1 µg/mL lipopolysaccharide (LPS; Sigma–Aldrich Co.) were used as positive controls for NO production.

Macrophage intracellular proteolysis

BMDM ($1x10^5$ cells/well) were plated in black clear bottom 96-well plates, maintained and infected as described above for the anti-amastigote activity assay. At 24 h after infection, cells were incubated with CH8 (1 µg/mL), LNC-CH8 or LNC for 20 min at 37°C. Then, cells were allowed to internalize the fluorogenic protein substrate DQ green-BSA (Thermo Fisher, UK) and human IgG (Sigma-Aldrich) - functionalized carboxylated silica beads (Kisker Biotech GmbH & Co., Germany) (5:1) for 5 minutes, as described previously[25]. Alexa Fluor 594 succidinimyl ester (Molecular Probes, USA) was used as a calibration fluorophore. After washing in PBS (to remove non-phagocytosed beads), the increase in fluorescence, indicative of proteolysis, was measured at different time points during a 2h period, at 37°C, using an FLX800 plate fluorimeter (BIO-

TEK, WI, USA) set at 594/620nm (for calibration fluorescence - CF) or 485/528nm (for substrate fluorescence - SF). The 'blank' (B) represented the cell fluorescence before treatment. The relative fluorescence (RF) was calculated as RF = (SF – B) / (CF – B).

Topical drug absorption assay

Mice were anesthetized with 2% isoflurane inhalation, and Rho-LNC-CH8 (20 µL, containing 11 µg of CH8) were applied to a shaved dorsal area of approximately 1.5 cm^2. At 0, 5, 15, 30, 60, 90, 120, 180, 240 and 300 min after application, fluorescence images of the whole animals were taken using an IVIS® Lumina Imaging System (Xenogen Corp, USA) with filters for rhodamine detection. A region of interest (ROI) was drawn 2 mm around the outer fluorescent margin, and the specific fluorescence was expressed as the difference between values for Rho-LNC-CH8 and LNC-CH8 surface radiance (photons/s/cm^2) for each time point. As a fluorescence quenching/decay control, the same amount of Rho-LNC-CH8 was applied per cm^2 onto an impermeable plastic blade and the fluorescence was measured as performed for animal skin.

Mouse infection and topical treatment

Mice were infected in the ear with $2x10^6$ promastigotes of *L. amazonensis*. On days 7 to 28 of infection, the ears were treated topically (5 times a week, using a disposable spatula) with one of the following formulations: (1) 10 µg of CH8 in PBS/2% DMSO (CH8 group); (2) 10 µg of CH8 in LNC-CH8) (LNC-CH8 group); blank LNC (LNC group); or 20 µL of 2% DMSO alone (untreated group). At the end of treatment (day 30 post-infection), the animals were euthanized by terminal 5% isoflurane inhalation, the infected ears were excised aseptically at the base, and homogenized individually in 1

mL of complete M199 medium. The parasite burden was evaluated by a limiting dilution assay (LDA), as described previously[26].

Statistical analysis

Data were analyzed by one-way or two-way ANOVA followed by Bonferroni multiple comparison test. Data were expressed as arithmetic mean ± standard deviation (SD) values and samples were considered significantly different when $p \leq 0.05$ in a series of at least three independent experiments.

RESULTS

3.1 LNC efficiently encapsulates CH8 into homogeneous nanoparticle suspensions.

All formulations were macroscopically homogeneous, and had unimodal narrow size dispersions, with mean diameters below 238 nm (laser diffraction) and 184 nm (PCS) (Table 1). All nanocapsules showed a slight negative zeta potential (ζ) close to zero (-6.1 to -7.5 mV). The drug content was close to 500 μg/mL with an encapsulation efficiency close to 100% (99.9%) (Table 1). Overall, nanocapsule sizes and surface potential were slightly affected by the drug loading or rhodamine labeling. The high efficiency of drug encapsulation corroborate the previous results observed for other drugs, such as doxorubicin, tacrolimus, quercetin, resveratrol and curcumin[16, 18, 27, 28].

3.2 Rho-LNC-CH8 is internalized by *L. amazonensis* promastigotes

To evaluate whether LNC could be internalized by parasite promastigote forms, these cells were incubated with Rho-LNC-CH8 (at 10 μg/mL of CH8) and the nanoparticle uptake was monitored over time, by flow cytometry and

fluorescence microscopy. Promastigotes internalized Rho-LNC-CH8 rapidly, and, within 15 minutes, a red fluorescence signal was observed in a specific sub-cellular compartment. Afterwards, at 60 min of internalization, the fluorescence signal appeared widespread in the cytoplasm. Quantification of the kinetics of Rho-LNC-CH8 internalization showed that the proportion of cells positive for Rho-LNC-CH8 increased with the incubation time (Figure 2), with ~80% of promastigotes having internalized Rho-LNC-CH8 by 60 min of incubation. These data showed the nanosystem is efficiently internalized by the *Leishmania* form that initiates infection in mammalian hosts.

3.3 CH8 encapsulation in LNCs did not decrease its anti-leishmanial activity.

In a previous study, we demonstrated that CH8 has potent and selective activity against *Leishmania* promastigotes[10]. Here, we tested both CH8 and LNC-CH8 against the intracellular forms of the parasite, the amastigotes. Infected macrophages were incubated with CH8, LNC-CH8 or LNC and the number of amastigotes inside host cells was assessed by direct counting under a light microscope, after 48 h of treatment (Table 2). Entrapping of CH8 in LNCs did not alter the anti-amastigote activity of the compound *in vitro*, as both CH8 and LNC-CH8 showed similar IC_{50} values (2.2 ± 0.1 and 2.9 ± 0.1 µg/mL, respectively). LNC (blank formulation) was not able to kill intracellular amastigotes (IC_{50} of 38.8 ± 0.3 µg/mL). However, LNC was not selective to the parasite, with encapsulation leading to a reduced selectivity index (SI) of CH8 towards the parasite, in comparison to the free drug.

3.4 LNC-CH8 delivers CH8 to *Leishmania* amastigotes inside host cells.

Since encapsulation on LNCs did not alter the activity of CH8 *in vitro*, we evaluated the internalization of Rho-LNC-CH8 by infected and uninfected macrophages, to verify if the nanocapsules could deliver CH8 effectively to parasites inside macrophages, where the parasite survives and multiplies. For this purpose, bone marrow-derived macrophages (BMDM) infected with *L. amazonensis* promastigotes expressing GFP[23] were incubated with Rho-LNC-CH8 (10 µg/mL CH8), and the internalization was evaluated at different time points (up to 240 min), by fluorescence microscopy and flow cytometry (Figure 3).

Similarly to that observed in promastigotes, Rho-LNC-CH8 was internalized quickly by infected and uninfected BMDMs, and we observed red fluorescence in the macrophage cytoplasm (but not in the nucleus) within 15 min of internalization (Figure 3A). In infected macrophages, the Rho-LNC-CH8 red fluorescence appeared faster (at 7.5 min) than in uninfected cells (Figure 3C), and internalization increased over time (Figure 3A and C). Importantly, the red fluorescence signal of Rho-LNC-CH8 was concentrated in the parasitophorous vacuole (PV) of infected cells (Figure 3A). Moreover, co-localization of Rho-LNC-CH8 with GFP-labeled amastigotes in the PV could be observed after 60 and 120 min of incubation. After 240 min of incubation, the Rho-LNC-CH8 fluorescence was found predominantly co-localized with GFP-labeled parasites in the PV, suggesting that Rho-LNC-CH8 had likely killed the amastigotes by that time point. In uninfected cells, the Rho-LNC-CH8 fluorescence signal had decreased by 240 min of internalization, with only low fluorescence being detected by fluorescence microscopy and a reduced

percentage of fluorescent cells detected by flow cytometry (Figure 3A, B and C). This decrease in fluorescence at later time points was not observed in infected cells (Figure 3C).

Together, these results confirm that LNC-CH8 can be internalized by infected macrophages and delivered to the PV, the intracellular compartment where the parasite is located.

3.5 LNC-CH8 triggers macrophage microbicidal mechanisms.

Phagocytes such as macrophages are capable of responding to infection by triggering microbicidal mechanisms, which include the production of reactive oxygen species (ROS) and nitric oxide (NO), and the activation of proteolytic enzymes and acidification of the PV. To study the influence of entrapment into LNCs on the activation of macrophage microbicidal mechanisms by CH8, we evaluated the stimulation of these mechanisms – which constitutes macrophage activation - in infected cells treated with LNC-CH8.

For ROS production, infected and uninfected macrophages were incubated with increasing concentrations of CH8, LNC-CH8 or LNC, and ROS production was assayed using the fluorescent dye H_2DCFDA (Figure 4, A and B). As expected, *Leishmania* infection decreased the basal ROS levels in untreated cells. CH8 was unable to activate ROS production in macrophages, even at high concentrations. In contrast, both LNC and LNC-CH8 induced ROS production at medium to high concentrations (Figure 4A and B).

In contrast, NO production (as estimated by $NaNO_2$ quantification in culture supernatants) increased only after treatment with high concentrations of

LNC-CH8; however, LNC and CH8 could not stimulate NO production, even at high concentrations (Figure 4C and D).

We assessed the proteolytic activity of macrophages by measuring the degradation of functionalized beads over time, in infected and uninfected cells treated with 1 µg/mL CH8, or equivalent amounts of LNC-CH8 and LNC. The proteolytic activity of uninfected cells was similar for all treatments (Figure 4E), while proteolysis levels increased over time in infected cells treated with LNC-CH8 or LNC, but not CH8 alone (Figure 4F). Although the proteolytic response was delayed in infected compared with uninfected cells, treatment of the former with LNC or LNC-CH8 eventually increased proteolysis levels above those observed uninfected cells (Figure 4F). CH8 encapsulation in LNC did not change cell acidification significantly (as assessed using the LysoTracker Green dye), irrespective of the presence of infection (data not shown).

The combined analysis of different antimicrobial mechanisms showed that LNC-CH8 can modulate host macrophage activation positively, which contributes to the activity of the LNC-CH8 nanosystem against the intracellular parasite.

3.6 Rho-LNC-CH8 is absorbed efficiently by mouse skin.

After the promising *in vitro* results described above, we evaluated if the LNC-CH8 formulation could permeate mouse skin and deliver the drug to macrophages *in vivo.* The kinetics of Rho-LNC-CH8 skin absorption was evaluated for up to 300 min after application onto the lightly shaved mouse hump. Although Rho-LNC-CH8 fluorescence was stable for up to 120 min after application, we observed a clear decrease in fluorescence thereafter until 240 min, when almost complete Rho-LNC-CH8 absorption was achieved (Figure 5A

and B). Spontaneous fluorescence quenching by drying was discarded by surface radiance quantification demonstrating that the fluorescence intensity of Rho-LNC-CH8 applied onto an impermeable plastic surface remained stable throughout the experiment (Figure 5B).

3.7 LNC-CH8 increased the efficacy of CH8 in cutaneous leishmaniasis treatment.

Given that Rho-LNC-CH8 is absorbed by mouse skin, we tested the activity of LNC-CH8 *in vivo* as a topical treatment for experimental CL, in BALB/c mice infected in the ear with GFP-labeled *L. amazonensis*.

After 3 weeks of daily topical treatment (5 days / week) with LNC, LNC-CH8 or CH8 (10 µg CH8 per cm^2/ dose), the parasite burden was evaluated in infected mouse ears by a limiting dilution assay. Mice treated with LNC-CH8 had significantly fewer parasites in infected ears than animals either treated with CH8 alone, or kept untreated (Figure 6). Thus, encapsulation of CH8 in LNC-CH8 increased its efficacy by the topical route in a murine model of CL.

DISCUSSION

In recent years, various topical formulations containing paromomycin, pentavalent antimonials, β-lapachone and amphotericin B have been developed for CL treatment[4-6, 29], but none were sufficiently effective or safe for clinical approval. Here, we evaluated the efficacy of a new topical nanoformulation against CL that combined the potency of a promising antileishmanial compound – the nitro-chalcone CH8[11] - with the skin permeation ability of the versatile LNC[30].

The results demonstrated that PCL and the oily component used here were adequate to provide a high rate of CH8 incorporation into LNC-CH8 (99.9%). Most of the drug was probably retained into the lipid compartment, which is protected by the PCL shell, thus increasing its bioavailability, as demonstrated for oral quercetin and resveratrol[16,31]. Despite their weak negative charge (-7.5 mV), LNC-CH8 stability was achieved by steric hindrance promoted by the nonionic polysorbate 80 surfactant[32].

The resulting LNC-CH8 were readily taken up by both macrophages and promastigote forms of *Leishmania*. Light microscopy analysis of Rho-LNC-CH8 internalization suggests that the nanocapsules enter promastigotes through the flagellar pocket and are transported to organelles of the endocytic pathway (likely corresponding to lysosome multivesicular tubules[33]) within 15 min, and then reach the cytoplasm. In macrophages, Rho-LNC-CH8 may reach the cytoplasm by fluid phase endocytosis, as described for LNC-doxorubicin[28]. Therefore, our data suggest that LNC-CH8 are only degraded after reaching the PV[34], where *Leishmania* amastigotes reside.

Encapsulation in LNC did not impair the anti-amastigote activity of CH8, as observed previously with poly(lactide-co-glycolide) (PLGA) microspheres that delayed intracellular parasite killing[22]. LNC may produce faster drug delivery to intracellular parasites due to their smaller size and/or higher sensitivity to lysosomal enzymes, compared with PLGA microspheres. The higher cytotoxicity of LNC-CH8 and LNC to macrophages, compared with CH8, is likely caused by the presence of polysorbate 80 surfactant in both LNC formulations. Despite the increased cytotoxicity, LNC-CH8 selectivity remained high - at 61 fold - which is comfortably above the 10-fold selectivity index advocated by

DNDi as a 'cut-off' for promising new antiparasitic drugs[35]. Additionally, the polysorbate 80 cytotoxicity observed here may not be relevant *in vivo*, especially for topical administration, since intradermal polysorbate 80-containing LNC systems are safe to rats[36].

The innate immune response to parasitic infection leads to the production of ROS and NO which together generate peroxynitrite (ONOO-), a strong oxidant considered essential for parasite killing by phagocytic cells[37]. These compounds can also increase the expression of genes associated with pro-inflammatory responses, such as NF-κB transcription factors[38]. While nanocarriers are known to activate these mechanisms,[39,40] the LNC nanoparticles used in this studies only led to an increase in ROS species. Moreover, in line with the antioxidant and anti-inflammatory effects of chalcones[40,41], CH8 alone could not activate macrophage antimicrobial mechanisms. in contrast, encapsulation into LNC led to ROS and NO production in both uninfected and infected cells. The former possibly accounting for the slightly increased macrophage cytotoxicity observed with LNC-CH8. Interestingly, intracellular *Leishmania* parasites downregulate these macrophage antimicrobial mechanisms[2] and the use of LNC nanocarriers may help to overcome this effect.

In addition to ROS and NO production, intracellular proteolysis is essential for microbial killing after endocytosis[42]. Interestingly, for safe therapeutic purposes, LNC-CH8 induced proteolytic activity in infected but not uninfected macrophages, suggesting that the presence of the parasites was necessary for the activation of cellular digestion mechanisms.

The lower efficacy of previous topical formulations for CL is possibly due to lack of proper drug permeation through the *stratum corneum* barrier of the skin, necessary to reach the infected cells in the lower dermis layer[30]. Despite its low molecular weight (329Da) and high lipophilicity (LogP = 3.63), CH8 alone cannot permeate the skin barrier[43]. However, the imaging studies shown here demonstrate that Rho-LNC-CH8 applied onto the mouse skin surface is no longer detectable 3 hours post-application, suggesting that the drug is absorbed efficiently by the skin. The time required for skin signal decrease suggests that drug absorption is not due to occlusion, as reported previously for solid lipid nanoparticles[44]. Rho-LNC-CH8 and LNC-CH8 permeation through skin appendages (hair follicles or sweat glands)[30] appears more plausible. This is agreement with the studies of Raber et al[45] demonstrating that negatively charged nanoparticles are able to interact more efficiently with the skin surface, facilitating follicular uptake.

Although the mechanism by which LNC-CH8 promotes drug permeation through the skin remains unclear, the *in vivo* data in murine CL clearly show that topical application of LNC-CH8 onto mouse lesions effectively reduced the parasite load by ~80% in comparison with free CH8. Interestingly, LNC alone reduced the number of parasites in skin lesions by ~30%. Although blank LNC does not have intrinsic antiparasitic activity, as seen by the lack of *in vitro* activity, our data suggest that this blank nanodevice is an excellent adjuvant for topical CL treatment. LNC-CH8 was more effective than other nanosystems attempted for CL topical treatment[29, 46]. Following the skin permeating potential demonstrated here, future LNC-CH8 manipulations may further improve its antiparasitic activity. One possibility is LNC co-entrapment with

superparamagnetic iron oxide nanoparticles (SPIONs) to allow heating and killing of the infected cells after local application of a magnetic field, as envisaged for cancer thermotherapy[47].

Overall, the results reported here show that LNC-CH8 is an appropriate nanosystem not only for intracellular drug delivery, but also for skin permeation and intracellular parasite killing. This study has clinical relevance for localized and safe treatment of CL, a skin pathology for which there is currently no adequate topical treatments.

ACKNOWLEDGEMENTS

The authors thank Bruna Donida for assisting with the quantification of CH8.

REFERENCES

1. Alvar J, Vélez ID, Bern C, et al. Leishmaniasis worldwide and global estimates of its incidence. *PloS one*. 2012; 7: e35671-e.
2. Moradin N and Descoteaux A. Leishmania promastigotes: building a safe niche within macrophages. *Frontiers in Cellular and Infection Microbiology*. 2012; 2: 121-.
3. de Menezes JPB, Guedes CES, Petersen ALdOA, Fraga DBM and Veras PST. Advances in Development of New Treatment for Leishmaniasis. *BioMed Research International*. 2015; 2015: 1-11.
4. Kim DH, Chung HJ, Bleys J and Ghohestani RF. Is Paromomycin an Effective and Safe Treatment against Cutaneous Leishmaniasis? A Meta-Analysis of 14 Randomized Controlled Trials. *PLOS Neglected Tropical Diseases*. 2009; 3: e381.
5. Sampaio RNR, Lucas IC and Takami HL. Inefficacy of the association N-methyl glucamine and topical miltefosine in the treatment of experimental cutaneous leishmaniasis by Leishmania (Leishmania) amazonensis. *Journal of Venomous Animals and Toxins including Tropical Diseases*. 2007; 13: 598-606.
6. López L, Vélez I, Asela C, et al. A phase II study to evaluate the safety and efficacy of topical 3% amphotericin B cream (Anfoleish) for the treatment of uncomplicated cutaneous leishmaniasis in Colombia. *PLOS Neglected Tropical Diseases*. 2018; 12: e0006653.
7. Brown MB, Martin GP, Jones SA and Akomeah FK. Dermal and Transdermal Drug Delivery Systems: Current and Future Prospects. *Drug Delivery*. 2006; 13: 175-87.
8. Williams AC and Barry BW. Penetration enhancers. *Advanced Drug Delivery Reviews*. 2012; 64: 128-37.
9. DNDi. DNDi's Strategy for Cutaneous Leishmaniasis.
10. Boeck P, Bandeira Falcão CA, Leal PC, et al. Synthesis of chalcone analogues with increased antileishmanial activity. *Bioorganic & medicinal chemistry*. 2006; 14: 1538-45.
11. Sousa-Batista AJ, Escrivani-Oliveira D, Falcao CAB, Philippon C and Rossi-Bergmann B. Broad spectrum and safety of oral treatment with a promising nitrosylated chalcone in murine leishmaniasis. *Antimicrobial agents and chemotherapy*. 2018.
12. Sousa-Batista AdJ, Pacienza-Lima W, Arruda-Costa N, Falcão CAB, Ré MI and Rossi-Bergmann B. Depot Subcutaneous Injection with Chalcone CH8-Loaded Poly(Lactic-Co-Glycolic Acid) Microspheres as a Single-Dose Treatment of Cutaneous Leishmaniasis. *Antimicrobial agents and chemotherapy*. 2018; 62: AAC.01822-17.
13. Sousa-Batista AJ, Arruda-Costa N, Rossi-Bergmann B and Ré MI. Improved drug loading via spray drying of a chalcone implant for local treatment of cutaneous leishmaniasis. *Drug Development and Industrial Pharmacy*. 2018; 0: 1-28.
14. Goyal R, Macri LK, Kaplan HM and Kohn J. Nanoparticles and nanofibers for topical drug delivery. *Journal of controlled release : official journal of the Controlled Release Society*. 2016; 240: 77-92.
15. Venturini CG, Jäger E, Oliveira CP, et al. Formulation of lipid core nanocapsules. *Colloids and Surfaces A: Physicochemical and Engineering Aspects*. 2011; 375: 200-8.
16. Sousa-Batista AJ, Poletto FS, Philipon CIMS, Guterres SS, Pohlmann AR and Rossi-Bergmann B. Lipid-core nanocapsules increase the oral efficacy of quercetin in cutaneous leishmaniasis. *Parasitology*. 2017: 1-6.
17. da Silva ALM, Contri RV, Jornada DS, Pohlmann AR and Guterres SS. Vitamin K1-loaded lipid-core nanocapsules: Physicochemical characterization and in vitro skin permeation. *Skin Research and Technology*. 2013; 19: e223-e30.
18. Friedrich RB, Kann B, Coradini K, Offerhaus HL, Beck RCR and Windbergs M. Skin penetration behavior of lipid-core nanocapsules for simultaneous delivery of resveratrol and curcumin. *European Journal of Pharmaceutical Sciences*. 2015; 78: 204-13.

19. NRC. *Guide for the Care and Use of Laboratory Animals*. 8th edition ed.: Washington (DC): National Academies Press (US), 2011.
20. Poletto FS, De Oliveira CP, Wender H, et al. How Sorbitan Monostearate Can Increase Drug-Loading Capacity of Lipid-Core Polymeric Nanocapsules. *Journal of Nanoscience and Nanotechnology*. 2015; 15: 827-37.
21. Poletto FS, Fiel La, Lopes MV, et al. Fluorescent-Labeled Poly(ε-caprolactone) Lipid-Core Nanocapsules: Synthesis, Physicochemical Properties and Macrophage Uptake. *Journal of Colloid Science and Biotechnology*. 2012; 1: 89-98.
22. Sousa-Batista AJ, Pacienza-Lima W, Arruda-Costa N, Falcão CAB and Rossi-Bergmann B. Depot subcutaneous injection with chalcone CH8-loaded PLGA microspheres aiming at a single-dose treatment of cutaneous leishmaniasis. *Antimicrobial agents and chemotherapy*. 2018; 62: 1-11.
23. Costa SdS, de Assis Golim M, Rossi-Bergmann B, Costa FTM and Giorgio S. Use of In Vivo and In Vitro Systems to Select Leishmania amazonensis Expressing Green Fluorescent Protein. *Korean J Parasitol*. 2011; 49: 357-64.
24. Granger DL, Taintor RR, Boockvar KS and Hibbs JB, Jr. Measurement of nitrate and nitrite in biological samples using nitrate reductase and Griess reaction. *Methods in enzymology*. 1996; 268: 142-51.
25. VanderVen BC, Hermetter A, Huang A, Maxfield FR, Russell DG and Yates RM. Development of a novel, cell-based chemical screen to identify inhibitors of intraphagosomal lipolysis in macrophages. *Cytometry Part A*. 2010; 77: 751-60.
26. Titus RG, Marchand M, Boon T and Louis JA. A limiting dilution assay for quantifying Leishmania major in tissues of infected mice. *Parasite Immunol*. 1985; 7: 545-55.
27. Friedrich RB, Coradini K, Fonseca FN, Guterres SS, Beck RCR and Pohlmann AR. Lipid-Core Nanocapsules Improved Antiedematogenic Activity of Tacrolimus in Adjuvant-Induced Arthritis Model. *Journal of nanoscience and nanotechnology*. 2016; 16: 1265-74.
28. Antonow MB, Asbahr ACC, Raddatz P, et al. Liquid formulation containing doxorubicin-loaded lipid-core nanocapsules: Cytotoxicity in human breast cancer cell line and in vitro uptake mechanism. *Materials Science and Engineering C*. 2017; 76: 374-82.
29. Moreno E, Schwartz J, Larrea E, et al. Assessment of β-lapachone loaded in lecithin-chitosan nanoparticles for the topical treatment of cutaneous leishmaniasis in L. major infected BALB/c mice. *Nanomedicine: Nanotechnology, Biology and Medicine*. 2015; 11: 2003-12.
30. Pohlmann AR, Detoni CB, Paese K, Coradini K, Beck RCR and Guterres SS. Polymeric Nanocapsules for Topical Delivery. In: Dragicevic N and Maibach HI, (eds.). *Percutaneous Penetration Enhancers Chemical Methods in Penetration Enhancement: Nanocarriers*. Berlin, Heidelberg: Springer Berlin Heidelberg, 2016, p. 201-21.
31. Detoni CB, Souto GD, da Silva ALM, Pohlmann AR and Guterres SS. Photostability and Skin Penetration of Different E-Resveratrol-Loaded Supramolecular Structures. *Photochemistry and Photobiology*. 2012; 88: 913-21.
32. Fiel LA, Rebelo LM, Santiago TD, et al. Diverse deformation properties of polymeric nanocapsules and lipid-core nanocapsules. *Soft Matter*. 2011; 7: 7240-7.
33. Waller RF and McConville MJ. Developmental changes in lysosome morphology and function Leishmania parasites. *International Journal for Parasitology*. 2002; 32: 1435-45.
34. Kou L, Sun J, Zhai Y and He Z. The endocytosis and intracellular fate of nanomedicines: Implication for rational design. *Asian Journal of Pharmaceutical Sciences*. 2013; 8: 1-10.
35. Don ROB and Ioset J-R. Screening strategies to identify new chemical diversity for drug development to treat kinetoplastid infections. *Parasitology*. 2014; 141: 140-6.
36. Bulcão RP, De Freitas FA, Dallegrave E, et al. In vivo toxicological evaluation of polymeric nanocapsules after intradermal administration. *European Journal of Pharmaceutics and Biopharmaceutics*. 2014; 86: 167-77.

37. Prolo C, Álvarez MN and Radi R. Peroxynitrite, a potent macrophage-derived oxidizing cytotoxin to combat invading pathogens. 2014, p. 215-25.
38. Hussain S, Garantziotis S, Rodrigues-Lima F, Dupret JM, Baeza-Squiban A and Boland S. Intracellular signal modulation by nanomaterials. *Advances in Experimental Medicine and Biology*. 2014; 811: 113-34.
39. Drewes CC, Fiel LA, Bexiga CG, et al. Novel therapeutic mechanisms determine the effectiveness of lipid-core nanocapsules on melanoma models. *International journal of nanomedicine*. 2016; 11: 1261-79.
40. Sökmen M and Akram Khan M. The antioxidant activity of some curcuminoids and chalcones. *Inflammopharmacology*. 2016; 24: 81-6.
41. Won S-J, Liu C-T, Tsao L-T, et al. Synthetic chalcones as potential anti-inflammatory and cancer chemopreventive agents. *European Journal of Medicinal Chemistry*. 2005; 40: 103-12.
42. Yates RM, Hermetter A and Russell DG. The kinetics of phagosome maturation as a function of phagosome/lysosome fusion and acquisition of hydrolytic activity. *Traffic*. 2005; 6: 413-20.
43. Rossi-Bergmann B, Falcão CAB, Zanchetta B, Badra Bentley MVL and Santana MHA. Performance of Elastic Liposomes for Topical Treatment of Cutaneous Leishmaniasis. In: Beck R, Guterres S and Pohlmann A, (eds.). *Nanocosmetics and Nanomedicines: New Approaches for Skin Care*. Berlin, Heidelberg: Springer Berlin Heidelberg, 2011, p. 181-96.
44. Puglia C and Bonina F. Lipid nanoparticles as novel delivery systems for cosmetics and dermal pharmaceuticals. *Expert Opinion on Drug Delivery*. 2012; 9: 429-41.
45. Raber AS, Mittal A, Schafer J, et al. Quantification of nanoparticle uptake into hair follicles in pig ear and human forearm. *J Control Release*. 2014; 179: 25-32.
46. Mohebali M, Rezayat MM, Gilani K, et al. Nanosilver in the treatment of localized cutaneous leishmaniasis caused by Leishmania major (MRHO/IR/75/ER): an in vitro and in vivo study. *2015*. 2015: 5.
47. Montazerabadi A, Beik J, Irajirad R, et al. Folate-modified and curcumin-loaded dendritic magnetite nanocarriers for the targeted thermo-chemotherapy of cancer cells. 2019; 47: 330-40.

FIGURE LEGENDS

Figure 1. Chemical structure of the chalcone CH8.

Figure 2. **Kinetics of Rho-LNC-CH8 internalization by promastigotes**. *Leishmania amazonensis* promastigotes were incubated with rhodamine-labeled LNC-CH8 (Rho-LNC-CH8, at 10 µg/mL CH8) and analyzed at different time points, to detect compound internalization. (A) Light microscopy analysis of live promastigotes, showing internalization of red-fluorescent Rho-LNC-CH8 from 0 to 60 min of incubation. DIC, differential interference contrast. Scale bar,

5 µm. (B, C) Flow cytometry analysis of the Rho-LNC-CH8 fluorescence intensity in promastigotes (10^5 events/sample) at different time points, displayed as histograms (B) and as the percentage of cells expressing > 6 x 10^0 arbitrary units of fluorescence (C; corresponding to cells in gate M1, in B). AU, arbitrary units. (n=3).

Figure 3. Rho-LNC-CH8 is efficiently internalized by macrophages. Bone marrow derived macrophages (BMDM) were infected with *L. amazonensis* expressing GFP and incubated with Rho-LNC-CH8 (10 µg/mL CH8). (A) Light microscopy analysis of uninfected and infected BMDM at different time points of incubation with Rho-LNC-CH8, showing co-localization between amastigotes (in green) and Rho-LNC-CH8 (in red), after 120 min of incubation. DIC, differential interference contrast. Scale bar, 20 µm. (B, C) Flow cytometry analysis of uninfected and infected BMDM after 240 min of Rho-LNC-CH8 internalization. The histograms in B show treated cells in blue, and untreated in grey, and the percentage of cells expressing >3 x 10^0 arbitrary fluorescence units (gate M1 in B) is shown in C (mean ± SD values, n=3 independent experiments). *$p<0.05$. AU, arbitrary units.

Figure 4. LNC-CH8 (but not CH8 alone) activates infected macrophages. Bone marrow derived macrophages (BMDM) were kept uninfected (A, C, E) or were infected with *L. amazonensis* (B, D, F), treated with LNC, CH8 or LNC-CH8 and then processed for the analysis of different markers of macrophage activation. (A, B) Reactive oxygen species (ROS) production was measured fluorimetrically using H_2DCFDA, after 30 min of treatment. FU, fluorescence units (C, D) Nitric oxide (NO) levels were estimated by quantifying $NaNO_2$ in culture supernatants (by the Griess method), after 48h of treatment. (E, F).

Intracellular proteolysis was assessed by using DQ green-BSA and IgG-functionalized beads, after 30 min of treatment. Results are expressed as relative fluorescence (RF). Data represent mean ± SD values (n=3 independent experiments). *p < 0.05, **p < 0.01, relative to free CH8.

Figure 5. Topical Rho-LNC-CH8 is absorbed through living mouse skin. Rhodamine-labeled CH8 (Rho-LNC-CH8, with 10 µg/mL CH8) was applied onto the pre-shaved dorsum of BALB/c mice and the skin fluorescence kinetics was followed by *in vivo* fluorescent imaging using the IVIS® Lumina system (A). A region of interest (ROI) was drawn 2 mm around the outer fluorescent margin, and data expressed as average surface radiance (photons/s/cm^2) after deduction of background fluorescence of skin to which unlabeled LNC-CH8 was applied (red line). As a control for fluorescence quenching/decay, the same amount of Rho-LNC-CH8 or LNC-CH8 was applied onto an impermeable surface (blue line) (B). Means ± SD values (n=5).

Figure 6. Efficacy of topical LNC-CH8 against cutaneous leishmaniasis. BALB/c mice were infected in the left ear with 2x10^6 promastigotes of *L. amazonensis.* Seven days after infection, the infected ears were treated topically once a day (five times a week), for 3 weeks, with 20 µL of LNC, LNC-CH8 containing 10 µg of CH8 (22.5 µg CH8 per cm^2) or the same amount of free CH8 in PBS/2% DMSO. The untreated group was administered only the drug-free vehicle. After 30 days of infection, animals were euthanized, the ears were removed and the parasite burden was quantified by a limiting dilution assay. Data represent mean ± SD values of one out of two independent experiments (n=5 animals/group). ** p<0.01.

Formulation	D[4,3] (nm)	SPAN	ζ (mV)	z-average diameter (nm)	PDI	CH8 content (μg/mL)	EE%
LNC	167 ± 0.009	1.20 ± 0.1	-6.10 ± 0.09	181± 09	0.12 ± 0.01	-	-
LNC-CH8	238 ± 0.010	0.81 ± 0.1	-7.50 ± 0.07	174 ± 07	0.10 ± 0.01	501 ± 0.02	99.9
Rho-LNC-CH8	145 ± 0.013	1.12 ± 0.1	-6.47 ± 0.08	184 ± 11	0.08 ± 0.02	550 ± 0.03	99.9

Table 1. Physicochemical features of the different nanocapsules.
LNC, "blank" LNC; LNC-CH8, LNC entrapping CH8; Rho-LNC-CH8, LNC-CH8 produced using a rhodamine(Rho)-labelled precursor. ζ, zeta potential; EE, Encapsulation Efficiency. (n=3).

Table 2. **Anti-Leishmania activity of LNC-CH8 *in vitro*.**

TREATMENT	ANTI-AMASTIGOTE IC_{50} (µg/mL)	CYTOTOXICITY CC_{50} (µg/mL)	SI
CH8	2.15 ± 0.14	393.72 ± 0.09	183.1
LNC	38.83 ± 0.29	247.90 ± 0.06	6.3
LNC-CH8	2.90 ± 0.15	178.60 ± 0.12	61.6

IC_{50}, anti-amastigote activity estimated by light microscopy. CC_{50}, cytotoxicity estimated by lactate dehydrogenase release. SI, selectivity index (SI = CC_{50}/IC_{50}). (n=3).

GRAPHICAL ABSTRACT

The antileishmanial drug candidate CH8 was encapsulated in lipid-core nanocapsules (LNC-CH8), to improve drug bioavailability for topical treatment of cutaneous leishmaniasis. LNC-CH8 were able to control the infection by penetrating mouse skin and delivering the drug to infected dermal macrophages.

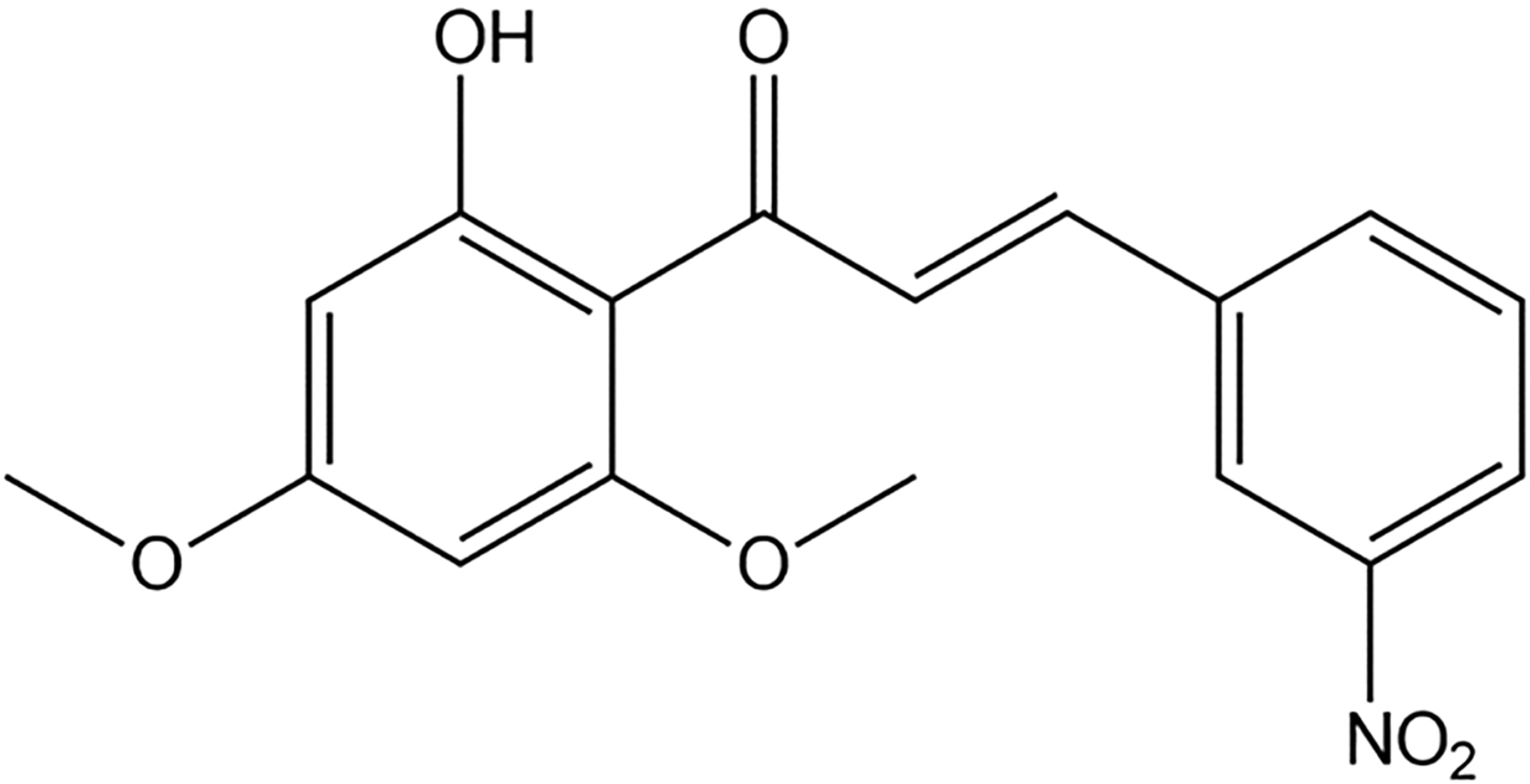

Figure 1

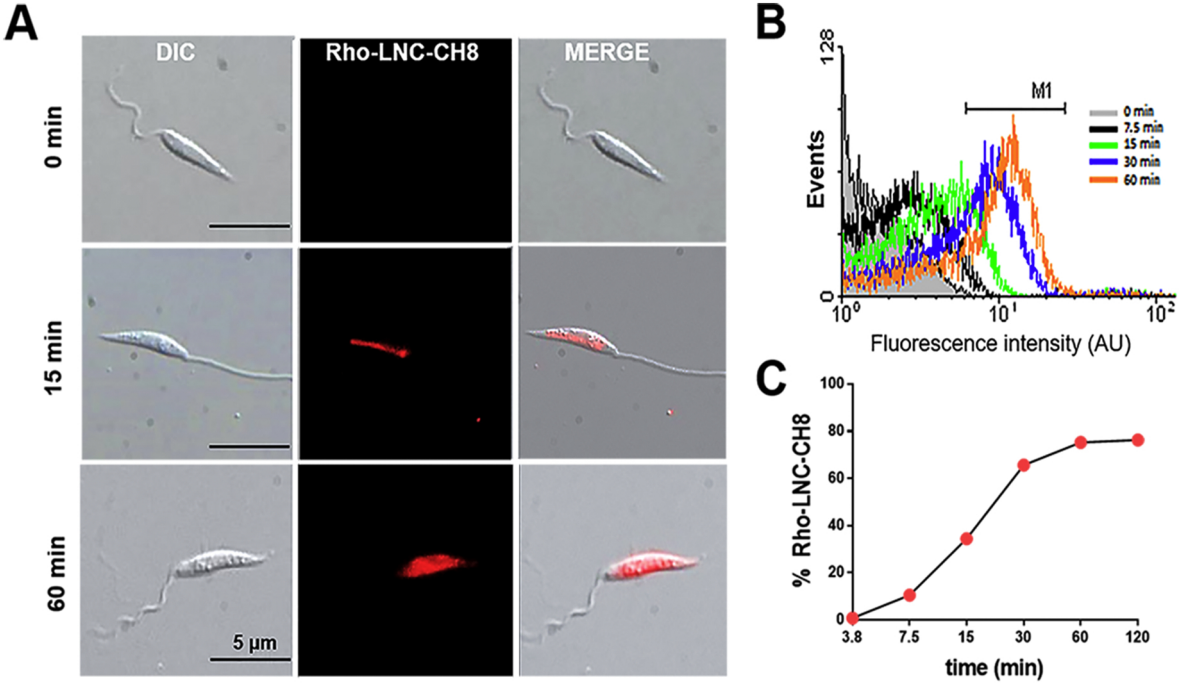
A
DIC
Rho-LNC-CH8
MERGE
0 min
15 min
60 min
5 µm
B
128
0
Events
M1
0 min
7.5 min
15 min
30 min
60 min
10^0
10^1
10^2
Fluorescence intensity (AU)
C
100
80
60
40
20
0
% Rho-LNC-CH8
3.8
7.5
15
30
60
120
time (min)

Figure 2

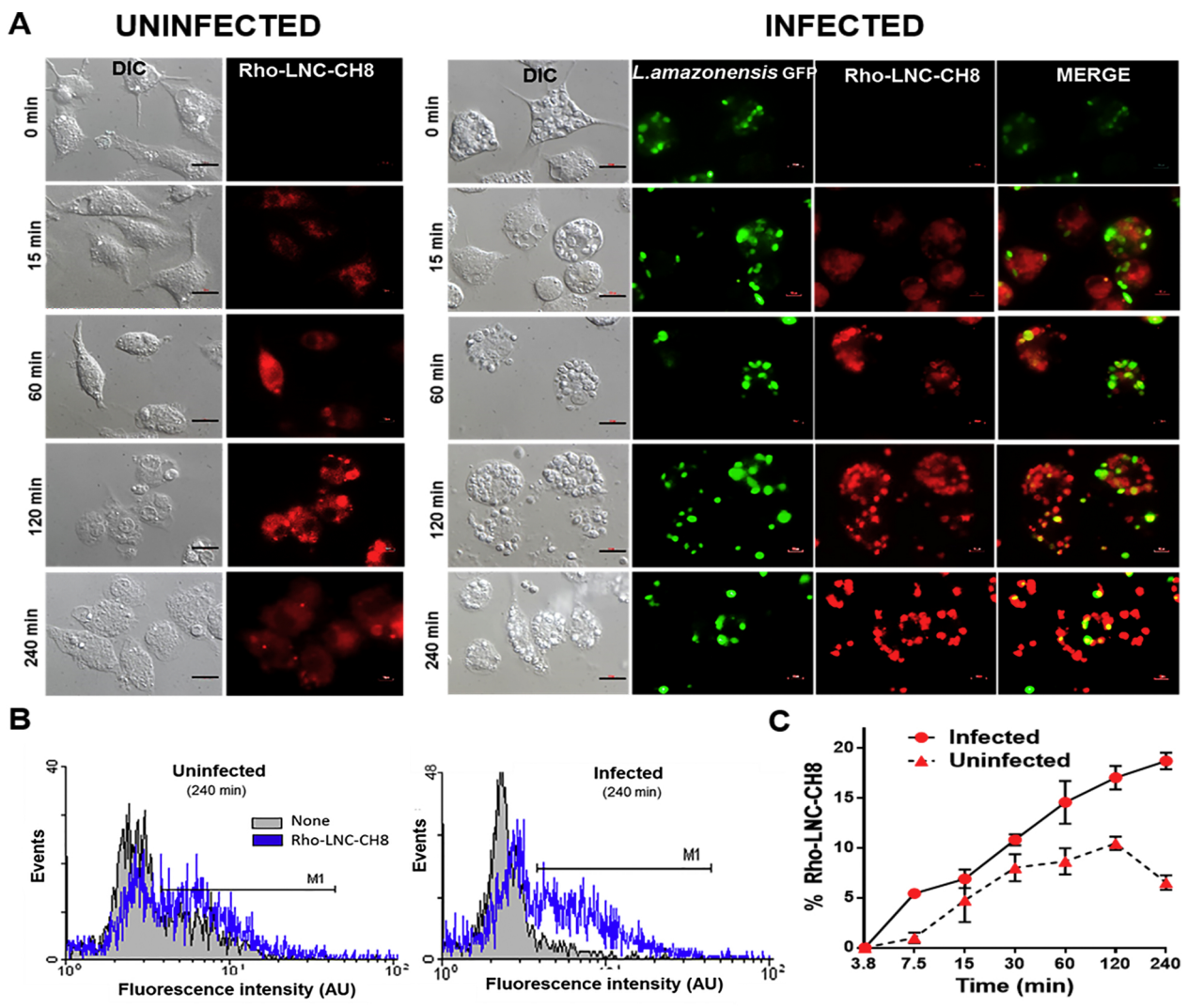
A
UNINFECTED
INFECTED
DIC
Rho-LNC-CH8
L.amazonensis GFP
MERGE
0 min
15 min
60 min
120 min
240 min
B
Uninfected
(240 min)
None
Rho-LNC-CH8
M1
Events
Fluorescence intensity (AU)
Infected
(240 min)
C
Infected
Uninfected
% Rho-LNC-CH8
Time (min)
3.8
7.5
15
30
60
120
240

Figure 3

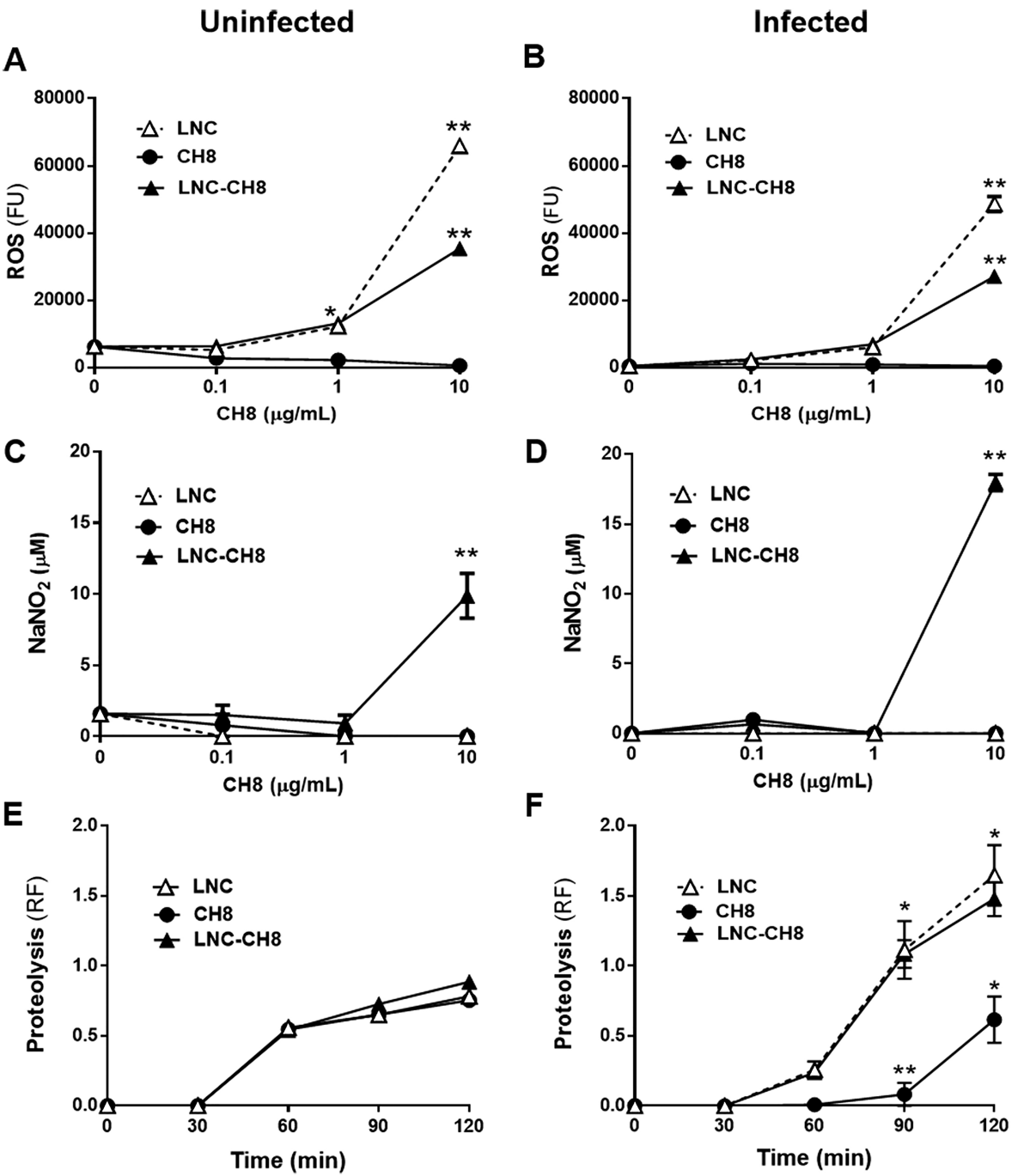
Uninfected
Infected
A
B
C
D
E
F
LNC
CH8
LNC-CH8
ROS (FU)
CH8 (μg/mL)
NaNO2 (μM)
Proteolysis (RF)
Time (min)
0
0.1
1
10
30
60
90
120
20000
40000
60000
80000
0.5
1.0
1.5
2.0
5
15
*
**

Figure 4

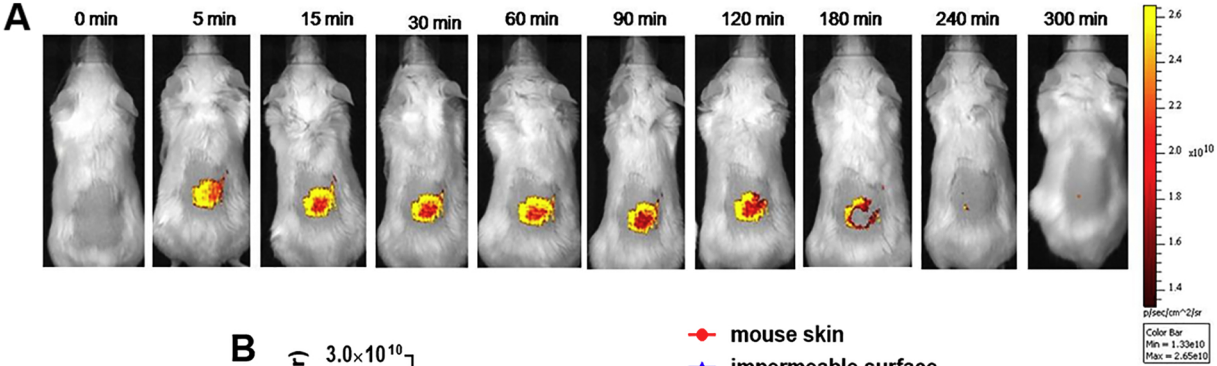
A
0 min
5 min
15 min
30 min
60 min
90 min
120 min
180 min
240 min
300 min
2.6
2.4
2.2
2.0 x10^10
1.8
1.6
1.4
p/sec/cm^2/sr
Color Bar
Min = 1.33e10
Max = 2.65e10
B
mouse skin
impermeable surface
Avg Radiance (p/s/cm2/sr)
3.0×10^10
2.0×10^10
1.0×10^10
0
0
100
200
300
Time (min)

Figure 5

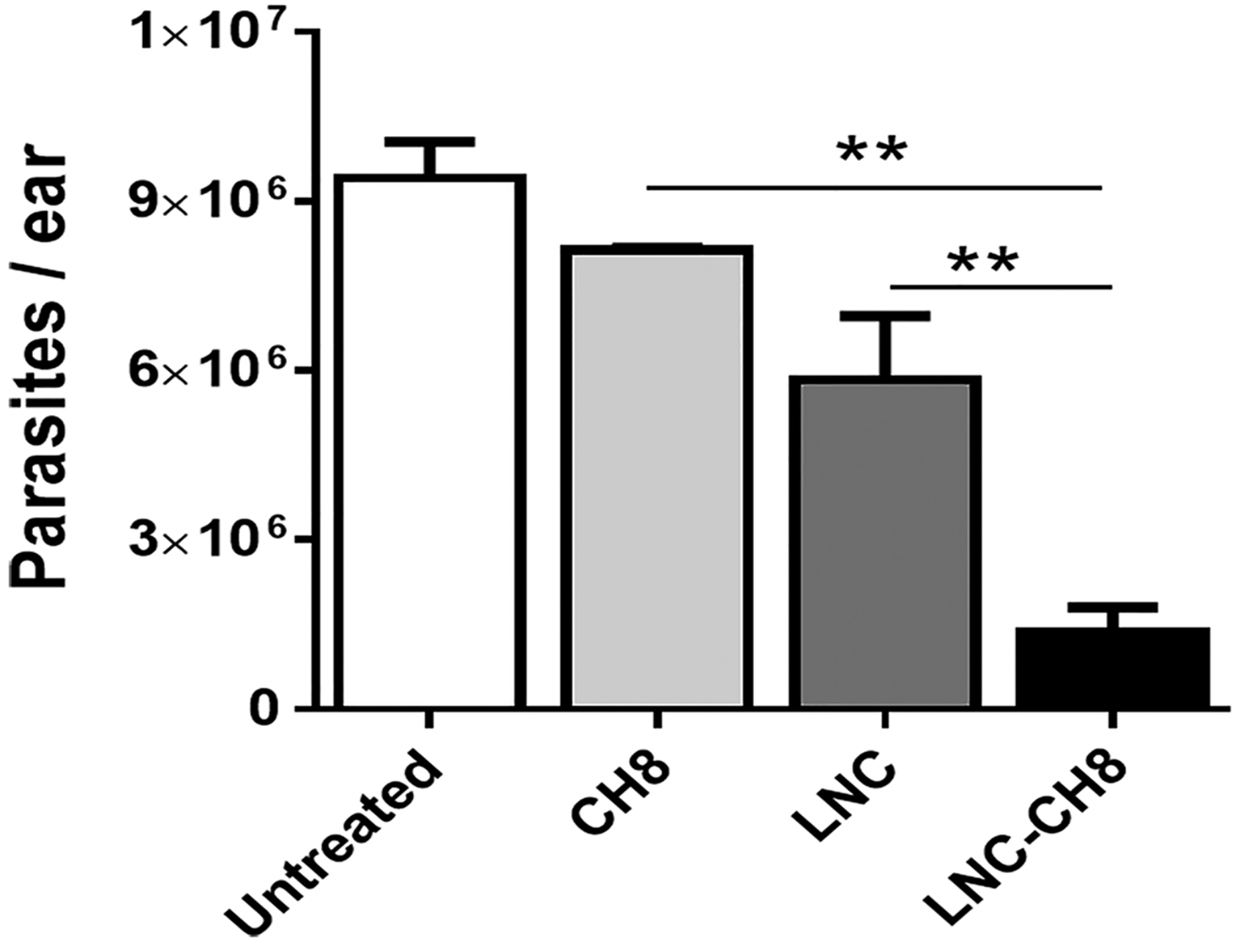
Parasites / ear
1×10^7
9×10^6
6×10^6
3×10^6
0
**
**
Untreated
CH8
LNC
LNC-CH8

Figure 6